AFRL-RW-EG-TP-2011-016

HAIR RECEPTOR SENSITIVITY TO CHANGES IN LAMINAR BOUNDARY LAYER SHAPE (POSTPRINT)

Benjamin T. Dickinson

Air Force Research Laboratory, Munitions Directorate
AFRL/RWGN
101 West Eglin Blvd
Eglin AFB, FL 32542

February 2010

AIR FORCE RESEARCH LABORATORY
MUNITIONS DIRECTORATE

■ **Air Force Materiel Command** ■ **United States Air Force** ■ **Eglin Air Force Base, FL 32542**

REPORT DOCUMENTATION PAGE

Form Approved
OMB No. 0704-0188

PLEASE DO NOT RETURN YOUR FORM TO THE ABOVE ADDRESS.

1. REPORT DATE *(DD-MM-YYYY)*	2. REPORT TYPE	3. DATES COVERED *(From - To)*
February 2010	Journal Article POSTPRINT	Sep 2008 - Feb 2010

4. TITLE AND SUBTITLE

Hair Receptor Sensitivity to Changes in Laminar Boundary Layer Shape

5a. CONTRACT NUMBER
N/A

5b. GRANT NUMBER
LRIR 09RWCOR

5c. PROGRAM ELEMENT NUMBER
61102F

6. AUTHOR(S)

B. T. Dickinson

5d. PROJECT NUMBER
2302

5e. TASK NUMBER
BW

5f. WORK UNIT NUMBER
98

7. PERFORMING ORGANIZATION NAME(S) AND ADDRESS(ES)

Air Force Research Laboratory, Munitions Directorate
AFRL/RWGN
101 West Eglin Blvd.
Eglin AFB, FL 32542

8. PERFORMING ORGANIZATION REPORT NUMBER
AFRL-RW-EG-TP-2011-016

9. SPONSORING/MONITORING AGENCY NAME(S) AND ADDRESS(ES)

Dr. Byung-Lip "Les" Lee
Air Force Office of Scientific Research
875 N Randolph Street
Arlington, VA 22203

10. SPONSOR/MONITOR'S ACRONYM(S)

11. SPONSOR/MONITOR'S REPORT NUMBER(S)

12. DISTRIBUTION/AVAILABILITY STATEMENT

DISTRIBUTION A. Approved for public release; distribution unlimited. 96 ABW/PA Approval and Clearance # 96ABW-2010-0084, dated 17 February 2010.

13. SUPPLEMENTARY NOTES

14. ABSTRACT

Biologists have shown that bat wings contain distributed arrays of flow-sensitive hair receptors. The hair receptors are hypothesized to feedback information on airflows over the bat wing for enhanced stability or maneuverability during flight. Here, we study the geometric specialization of hair-like structures for the detection of changes in boundary layer velocity profiles (shapes). A quasi-steady model that relates the flow velocity profile incident on the longitudinal axis of a hair to the resultant moment and shear force at the hair base is developed. The hair length relative to the boundary layer momentum thickness that maximizes the resultant moment and shear-force sensitivity to changes in boundary layer shape is determined. The sensitivity of the resultant moment and shear force is shown to be highly dependent on hair length. Hairs that linearly taper to a point are shown to provide greater output sensitivity than hairs of uniform cross-section. On an order of magnitude basis, the computed optimal hair lengths are in agreement with the range of hair receptor lengths measured on individual bat species. These results support the hypothesis that bats use hair receptors for detecting changes in boundary layer shape and provide geometric guidelines for artificial hair sensor design and

15. SUBJECT TERMS

Mechanoreceptor, Artificial Hair Sensor, Medium Flow Sensor

16. SECURITY CLASSIFICATION OF:			17. LIMITATION OF ABSTRACT	18. NUMBER OF PAGES	19a. NAME OF RESPONSIBLE PERSON
a. REPORT	b. ABSTRACT	c. THIS PAGE			Benjamin T. Dickinson
UNCLAS	UNCLAS	UNCLAS	UL	11	19b. TELEPHONE NUMBER *(Include area code)* 850-883-2645

Reset

Standard Form 298 (Rev. 8/98)
Prescribed by ANSI Std. Z39.18

Bioinsp. Biomim. **5** (2010) 016002 (11pp) doi:10.1088/1748-3182/5/1/016002

Hair receptor sensitivity to changes in laminar boundary layer shape

B T Dickinson

Air Force Research Laboratory, Munitions Directorate, Eglin Air Force Base, FL 32542, USA

E-mail: btdickinson@lifetime.oregonstate.edu

Received 14 September 2009
Accepted for publication 28 January 2010
Published 16 February 2010
Online at stacks.iop.org/BB/5/016002

Abstract
Biologists have shown that bat wings contain distributed arrays of flow-sensitive hair receptors. The hair receptors are hypothesized to feedback information on airflows over the bat wing for enhanced stability or maneuverability during flight. Here, we study the geometric specialization of hair-like structures for the detection of changes in boundary layer velocity profiles (shapes). A quasi-steady model that relates the flow velocity profile incident on the longitudinal axis of a hair to the resultant moment and shear force at the hair base is developed. The hair length relative to the boundary layer momentum thickness that maximizes the resultant moment and shear-force sensitivity to changes in boundary layer shape is determined. The sensitivity of the resultant moment and shear force is shown to be highly dependent on hair length. Hairs that linearly taper to a point are shown to provide greater output sensitivity than hairs of uniform cross-section. On an order of magnitude basis, the computed optimal hair lengths are in agreement with the range of hair receptor lengths measured on individual bat species. These results support the hypothesis that bats use hair receptors for detecting changes in boundary layer shape and provide geometric guidelines for artificial hair sensor design and application.

(Some figures in this article are in colour only in the electronic version)

1. Introduction

The unique physiology of bat wings aerodynamically distinguishes bat flight from the flight of birds by extreme maneuverability and greater flight efficiency. Metabolic studies show that bats require 20–25% less power for flight than birds [1]. Bats are also capable of performing 180° turns in narrow spaces at a rate of over 200° s^{-1} [2]. Such flight performance is linked to a highly anisotropic wing membrane [3, 4] that is articulated by more than two dozen joints [5, 6] and supported by compliant bones of an elongated bony hand and arm [4, 7]. A growing body of evidence also suggests that bat flight is enhanced through the feedback of airflow information over the bat wing from distributed mechanosensory wing hair receptors [8–10] (figure 1). In this work, we show that optimal hair lengths for detecting changes in a laminar boundary layer velocity profile (boundary layer shape) agrees with the lengths of bat wing hair receptors.

The sensing role of bat wing hair receptors is distinguished from pelage hair by their growth from dome-shaped complexes [8, 9, 11] and relatively smaller hair geometry (on the order of 100–1000 μm in length and 10 μm in diameter [11]). Hair receptor distribution and size vary among bat species, but are typically found near innervated elastin-collagen bands that span the wing membrane [9, 12]. Under the general idea that bat wing hair receptors are used for airflow feedback, hair receptors are thought to be specialized for both boundary layer detection [9] and the detection of a flow structure known as the leading edge vortex [10]. Here, we explore how hair-like structures may have adapted geometrically for the detection of changes in boundary layer shape. Specifically, we ask: what hair length(s), relative to the boundary layer thickness, *optimizes* the detection of changes in the boundary layer shape?

This research question is motivated, in part, by an apparent correlation between the length of hair receptors of spiders (trichobothria, 100–1400 μm) and the estimated boundary layer thicknesses over their bodies due to high-frequency

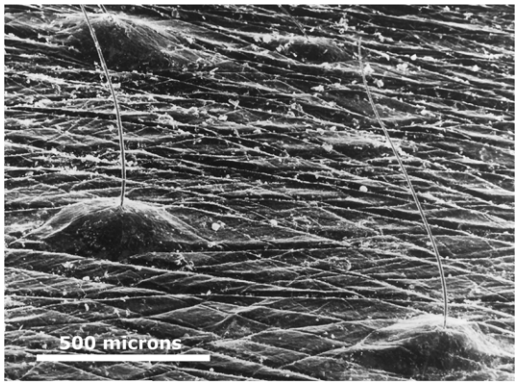

Figure 1. Scanning electron micrograph of wing hair receptors of the gray-headed flying fox (Pteropus *poliocephalus*). Reproduced with permission from G V Crowley and L S Hall 1994 *Aust. J. Zool.* **42** 215–231. © CSIRO 1994. Published by CSIRO PUBLISHING, Melbourne Australia—available at www.publish.csiro.au/nid/90/paper/ZO9940215.htm.

flows of nearby prey (600 μm at 950 Hz to 2600 μm at 600 Hz) [13–15]. Flow-sensitive hair-like structures on aquatic arthropods are similarly proportional to estimates of the boundary layer thicknesses over their bodies [14]. Barth *et al* provided numerical evidence suggesting that the scaling of hair receptor length with boundary layer thickness is adaptation for maximum hair deflection in oscillating flows due to nearby prey [13, 16].

In contrast to previous hair receptor studies concerning prey detection, we investigate bat wing hair receptors from the perspective of aerodynamic feedback. Thus, instead of studying hair sensors in oscillating flows over a range of frequencies modeled after nearby prey, we focus on flows with a bulk direction driven by various pressure gradients and intended to represent changing flight conditions. Despite the qualitative differences of these flow scenarios however, from the viewpoint of the boundary layer, these flows only differ by the sets of boundary layer shapes they provide. To this end, if fluctuations in boundary layer shape are a driving force behind the adaptation of hair receptors, differences in hair length (and potentially hair shape) may be an outcome of differences in the set of boundary layer shapes for which the hairs have evolved to sense.

Based on boundary layer fluctuations, bats could sense the state of the flow above their wings to enhance flight. Numerical studies show that the mechanical response of hair arrays provides a time and space accurate representation of boundary layer development and flow separation over a cylinder [17, 18]. For engineering applications, the detection of boundary layer shape with artificial hair sensors (AHS) may also provide a means of quantifying wall shear stress. Furthermore, wall shear measurements provided by AHS would have immediate relevance to previous boundary layer control designs where flow disturbances are effectively suppressed (to prevent turbulence) with wall shear feedback [19–21]. Multiple point-wise wall shear stress measurements with AHS may also provide estimates for the instantaneous skin-friction drag over body.

Wing hair receptor arrays for airflow feedback in bats inspire the use of AHS for micro-air-vehicles [17, 22]. Similarly, flow sensitive hair arrays found on the bodies of fish and implicated in their locomotion [23] inspire the application of AHS to underwater vehicles [24]. In both engineering applications, low-Reynolds number regimes (on the order of 10^5 or less) challenge vehicle stability, maneuverability or overall efficiency through unsteady aerodynamic or hydrodynamic forces. As low-Reynolds number animals (e.g. bats and fish) may use hair receptors as part of a feedback control loop, AHS could play a similar role in low-Reynolds number vehicles. For bats, one means of control (actuation) is simply changing the shape or kinematics of its wings during flapping flight. MAV actuators include the typical aircraft control surfaces (ailerons, rudders, elevators and flaps) and wing morphing [25].

Starting with the existing hypothesis that bats use hair receptors for boundary layer feedback, we consider hair-like structures as sensors of changes in boundary layer shape. Specifically, we will (1) determine a hair length to boundary layer thickness ratio, for hairs of uniform and linearly tapered cross-section, that maximizes hair sensitivity to changes in laminar boundary layer shape (2) show that hair length is a critical parameter for detecting changes in laminar boundary layer shape (3) show that hair shape can affect hair output sensitivity and (4) show that the range of optimal hair lengths for the detection of changes in boundary layer shape agrees with the range of bat wing hair receptor lengths.

The rest of this paper is organized as follows. In section 2, we develop a quasi-steady hair receptor model that describes the relationship between the flow velocity profile acting normal to the longitudinal axis of a hair and the resultant moment and shear force at the hair base. The underlying assumptions behind the hair model development are also discussed. In section 3, maps of hair outputs (resultant moment and shear stress) as a function of relative hair length (with respect to boundary layer momentum thickness) and boundary layer shape are presented for hairs of both uniform and linearly tapered cross-section. Measures of hair output sensitivity with respect to boundary layer velocity profile are then defined and relative hair lengths of maximum sensitivity are determined. Based on the optimized relative hair lengths for linearly tapered hairs, the range of dimensional optimal hair lengths over a bat wing are estimated and compared to biological data (section 3.3). Finally, a summary of this work and its implications is provided in section 4.

2. Hair receptor model

Our goal in modeling the hair receptor is to develop a relationship between the transverse forces due to the flow velocity profile incident on the longitudinal axis of the hair, further referred to as the *input*, and the resultant moment and shear force at the base of the hair, further together referred to as the *output* (figure 2). This choice of output was made for simplicity and generality of this analysis for both artificial and biological flow-sensitive hairs.

Implicit in our choice of hair output is the assumption that the resultant moment and shear force at the base of the hair are

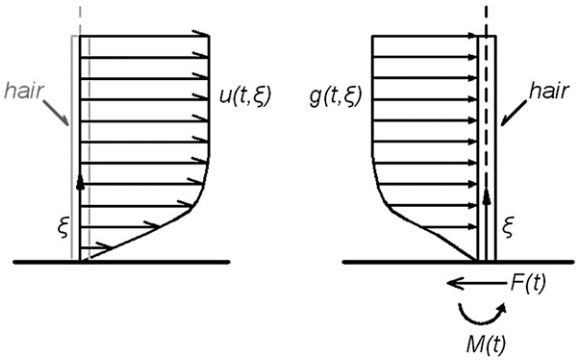

Figure 2. Nonuniform flow velocity profile incident on hair receptor (*left*) and corresponding free body diagram of hair (*right*).

related to afferent bioelectric signals of the actual hair receptor. We note that our choice of output differs from previous studies, which use hair displacement to interpret hair response [13–15, 26, 27]. The differences in sensor output quantities are due to differences in the mathematical models, which appear to stem from morphological differences between the structural support of bat wing hair receptors and arthropod trichobothria. Specifically, the shaft of bat hair receptors appears tightly enveloped by the dome complex (see figure 1 and [9]) leading to a rigid support in our hair model, while the shaft of spider trichobothria extends into a cup-like structure and is supported by a membrane at the cup base [13, 16], leading to a hair model with a pin support about which the hair may rotate.

We begin our model development by considering the forces in the airflow over a hair. Let the Reynolds number for flow normal to the hair longitudinal axis be defined as

$$Re_0 = \frac{U\, d_0}{\nu} \tag{1}$$

where U is a characteristic flow velocity, d_0 is a hair diameter and ν is the kinematic viscosity of air[1]. Characteristic speeds of bat and MAV flight range from $\sim 10^0$ to 10^1 m s^{-1}, based on flight Reynolds number estimates of $\sim 10^4$ to 10^5 with a characteristic wing length of $\sim 10^{-1}$ m (here, we use the symbol $\sim$ to denote orders of magnitude) [29]. Setting $U = 1$ to 10 m s^{-1}, and $d_0 = 10^{-5}$ m, a characteristic diameter of bat hair receptors[2] [11] gives $Re_0 = 0.63$–6.3. Although not a Stokes flow environment, the low Reynolds numbers indicate the importance of viscous forces in the airflow over the hair. Previous studies have also found that the viscous flow environment is the dominating influence that drives hair motion (see [30, 31] or [32] and the references therein). This implies that the relative importance of hair inertial forces is small. Humphrey *et al* have supported this implication whereby comparing the motion of solid and hollow hairs showed that the reduction in hair mass had a small effect on hair motion [26].

Relative hair motion with respect to the direction of the incident airflow may also affect the surface forces acting on the hair by creating a net drag force. The significance of the relative hair velocity on the drag force experienced by the hair may be assessed by comparing the time scales of the hair and flow velocity.

The time scale of the hair due to an applied stress may be estimated with the ratio of the coefficient of material damping, γ (N s m^{-2}), to the modulus of elasticity, E (N m^{-2}) [33], where the values of γ and E must be experimentally determined. Bat hair receptors are likely composed of alpha-type keratin, as is all mammalian hair. Although the material properties of bat hair receptors have yet to be identified, the dynamic time scales of alpha-type keratin wool fibers reportedly range from $\sim 10^1$ to 10^5 s, depending on the relative humidity of air [34].

As a time scale of the transverse forces on the hair due to the transverse flow velocity, we take the ratio of the characteristic hair diameter, d_0, to the characteristic flow velocity U, d_0/U. Using the values for d_0 and U reported above, the micro-scale hair diameter leads to $d_0/U \sim 10^{-6}$ to 10^{-5} s. Comparing the flow and material time scales, it is clear that

$$\frac{\gamma}{E} \gg \frac{d_0}{U}.$$

To this end, the hair is effectively motionless from the perspective of the flow and will exhibit quasi-steady behavior. Furthermore, since the flow time scale is very small, we anticipate that a quasi-steady assumption will be applicable for a wide variety of artificial hair materials. However, we note that model parameter estimates of spider and cricket hair receptor data [15] indicate time scales of $\sim 10^{-5}$ to 10^{-3} s. For these animals, the quasi-steady assumption may not be valid.

We also assume that throughout this analysis, the maximum hair tip deflection will be less than 10% of its length. This ensures that despite hair bending, a small angle approximation to the velocity profile incident normal to the undeflected hair will be valid. To test this assumption we performed a finite element analysis of a static Euler–Bernoulli beam (similar to the work in [22]), 1 m from the leading edge of a plate subject to the Blasius boundary layer with external flow of 10 m s^{-1}, hair length equal to the boundary layer thickness, a diameter 1% of its length (6.2×10^{-5} m) and modulus of elasticity of 2.0 GPa (representative of nylon). The resulting tip deflection was 7.1% of the hair length.

The statically determinate situation of the hair (figure 2), where maximum deflection is less than 10% of its length and the quasi-steady assumption, leads to the following expressions for resultant moment and shear force:

$$M(t) = \int_0^\ell g(t,\, \xi)\, \xi \, \mathrm{d}\xi \tag{2}$$

and

$$F(t) = \int_0^\ell g(t,\, \xi)\, \mathrm{d}\xi. \tag{3}$$

where $g(t,\, \xi)$ is the instantaneous load intensity that acts normal to the longitudinal axis having units of force per unit length.

For hairs with circular cross-section, we approximate the load intensity at any longitudinal position, ξ, along the hair as

$$g(t, \xi) = \tfrac{1}{2}\, C_d(Re_\xi)\, \rho\, d(\xi)\, u(t, \xi)^2 \tag{4}$$

[1] Evaluated at 300 K, as are all intensive flow properties herein.

[2] Based on data provided by Cynthia Moss of The Auditory Neuroethology Laboratory at The University of Maryland.

for $0 \leqslant \xi \leqslant \ell$ where ℓ is the hair length, ρ is the fluid density, d is the hair diameter, u is the flow velocity incident on the longitudinal axis and C_d is the drag coefficient for long ($\ell/d > 100$) circular cylinders in cross-flow. Due to the nonuniform boundary layer profile and a potentially nonuniform hair diameter, the drag coefficient, C_d, is determined as a function of the local Reynolds number,

$$Re_\xi = \frac{u(t,\xi)\, d(\xi)}{\nu}, \tag{5}$$

using a least-squares fit to empirical data [35] for drag coefficients of long circular cylinders in cross-flow at $Re_\xi = 10^{-1}$, 10^0 and 10^1. An R-squared value of 0.996 is obtained with the following linear logarithmic expression:

$$\log C_d = -\tfrac{2}{3}\, \log Re_\xi + \tfrac{5}{2}. \tag{6}$$

Note that the use of the drag coefficient in the expression for the load intensity (4) does not account for flow phenomena due to its free end or the surface where the hair is mounted. For long hairs, $\ell/d > 100$, we expect that end effects will have negligible contribution to the hair output. This condition holds throughout this analysis, except when hair length is much less than the boundary layer thickness.

When the expression for load intensity (4) is substituted into the equations for resultant moment (2) and shear (3), we obtain

$$M(t) = \int_0^\ell \frac{1}{2}\, C_d(Re_\xi)\, \rho\, d(\xi)\, u(t,\xi)^2\, \xi\, \mathrm{d}\xi \tag{7}$$

and

$$F(t) = \int_0^\ell \frac{1}{2}\, C_d(Re_\xi)\, \rho\, d(\xi)\, u(t,\xi)^2\, \mathrm{d}\xi. \tag{8}$$

Equations (7) and (8) relate the velocity profile of a viscous incompressible flow normal to the longitudinal axis of a hair-like structure having circular cross-section to the mechanical response at its base.

Although equations (7) and (8) are very simple in construction, our previous numerical studies show that the input–output relationship described by a linearized form of (7) agrees with flexible cantilever beam models responding to unsteady flows [17]. Furthermore, prior studies have shown that the resultant moment at the base of the hair provides a time accurate representation of the incident flow profile direction and magnitude, despite a wide range of hair motions (produced by assigning various material properties) that are out of phase with the incident flow [18]. In the following section we proceed with a nondimensionalization of equations (7) and (8) to length and velocity scales of the boundary layer.

2.1. Nondimensional form of hair model

For a general analysis within the context of boundary layer flows, we now recast equations (7) and (8) with the following nondimensional variables:

$$d^* = \frac{d}{d_0}, \qquad \xi^* = \frac{\xi}{\delta_2}, \qquad \ell^* = \frac{\ell}{\delta_2}, \qquad u^* = \frac{u}{U}, \tag{9}$$

where d_0 is a characteristic hair diameter (taken here as the base diameter $d(\xi = 0) = d_0$), δ_2 is the boundary layer momentum thickness and U is the external flow velocity.

The application of (9) to the resultant moment (7) results in an equivalent expression that is the product of a nondimensional coefficient of moment,

$$C_m = \frac{1}{\ell^{*2}} \int_0^{\ell^*} C_d(u^*, d^*, Re_0)\, d^*\, u^{*2}\, \xi^*\, \mathrm{d}\xi^*, \tag{10}$$

the dynamic pressure, $Q = \frac{1}{2}\, \rho\, U^2$, the frontal area, $A = d_0\, \ell$, and the characteristic length, ℓ, as

$$M(t) = C_m\, Q\, A\, \ell. \tag{11}$$

With a similar application of the nondimensional scales in (9) to the resultant shear force (8) we obtain the product of a nondimensional coefficient of shear force,

$$C_s = \frac{1}{\ell^*} \int_0^{\ell^*} C_d(u^*, d^*, Re_0)\, d^*\, u^{*2}\, \mathrm{d}\xi^*, \tag{12}$$

the dynamic pressure, Q, and frontal area, A, as

$$F(t) = C_s\, Q\, A. \tag{13}$$

The coefficients of moment (10) and shear force (12) are primarily a function of the nondimensional variables u^*, d^* and ℓ^* and are secondary functions of the reference Reynolds number, Re_0 (1). The dependence on Re_0 is obtained by applying (9) to local Reynolds number (5) as $Re_\xi = u^*\, d^*\, Re_0$.

2.2. Boundary layer model

In this section, we introduce the Falker–Skan boundary layer model and describe various measures of boundary layer thickness. The reader already familiar with these topics may skip this section without loss of continuity.

Computing hair output sensitivity requires an adequate description of changes in boundary layer shape. Here, we chose the Falkner–Skan equation which describes laminar boundary layer flows over a wedge (accelerated flows), corner (retarded flows) and flat plate (Blasius flow). The Falker–Skan equation is obtained from Prandtl's boundary layer equations with the assumption of self-similar solutions and is written as

$$\begin{gathered} f''' + f\, f'' + \beta\,(1 - f'^2) = 0, \\ f(0) = f'(0) = 0, \\ f'(\eta \to \infty), = 1 \end{gathered} \tag{14}$$

where $f = f(\eta)$ is a similarity variable, $f' = u^* = u/U$ is the nondimensional flow velocity profile, $\eta = y/\delta$ is a dimensionless wall normal coordinate and U is the uniform flow above the boundary layer. The boundary layer thickness measure, δ, is

$$\delta = \sqrt{\frac{2}{m+1}\, \frac{\nu\, x}{U}} \tag{15}$$

where $m = \beta/(2 - \beta)$ and the parameter β determines the corresponding geometry of the flow (i.e. plate, corner, wedge, etc), or equivalently the pressure gradient.

Since no analytical solution of (14) is known, solutions of the Falkner–Skan equation must be approximated numerically.

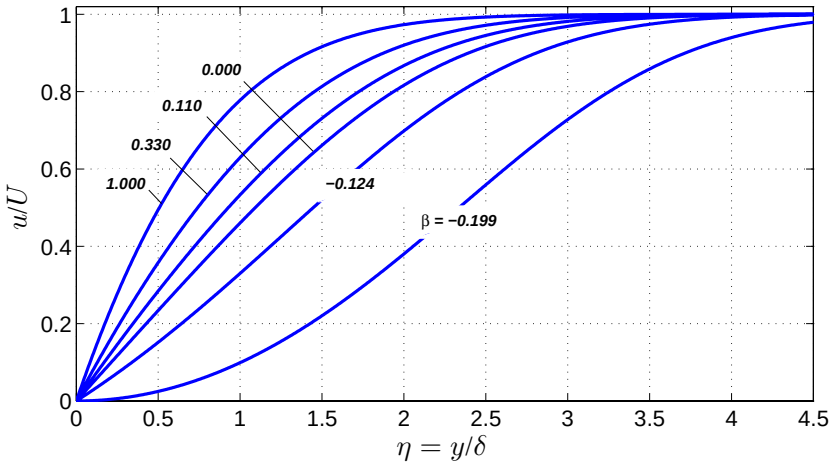

Figure 3. Solutions of the Falkner–Skan equation ranging from separation ($\beta = -0.199$) to plane stagnation ($\beta = 1.0$).

Here, we used a second-order accurate central-difference scheme known as the Keller box-method [36]. Figure 3 contains grid independent boundary layer profiles from the solution of (14) for β ranging from $\beta = -0.199$ (separation over a corner) to $\beta = 1.0$ (flow to a plane stagnation point).

Boundary layer shapes, such as those shown in figure 3, are further quantified herein with the Hartree shape factor,

$$H = \frac{\delta_1}{\delta_2},$$

where δ_1 is displacement thickness,

$$\delta_1 = \int_0^\infty \left(1 - \frac{u}{U}\right) \mathrm{d}\eta,$$

and δ_2 is the momentum thickness:

$$\delta_2 = \int_0^\infty \frac{u}{U}\left(1 - \frac{u}{U}\right) \mathrm{d}\eta.$$

The displacement and momentum thicknesses are well-defined quantities in laminar boundary layer flows. They are defined as the equivalent thickness of a flow layer having the external flow velocity, U, that accounts for the reduction in mass flow and momentum due to the presence of the boundary layer, respectively. The boundary layer thickness, δ_{99}, is also used herein and is defined as the height above the wall at which the horizontal velocity component reaches 99% of U.

In terms of the Hartree shape factor, $H = 4.029$ ($\beta = -0.199$) represents laminar separation, $H = 2.591$ ($\beta = 0.000$) corresponds to Blasius flow (flow over a flat plate) and $H = 2.216$ ($\beta = 1.000$) indicates flow to a plane stagnation point (Heimenz flow). For more information on boundary layer flows, see Schlichting and Gersten [37].

3. The optimal hair length for detecting changes in boundary layer shape

Any portion of a hair protruding from the boundary layer will have a corresponding contribution to its output represented by the external flow. Hairs that extend too far into the external flow will be less sensitive to changes in the boundary layer. Conversely, as hair length approaches zero, hair output and therefore output sensitivity approaches zero. Thus, for maximum output sensitivity to changes in boundary layer shape we propose that the hair length be limited by a measure of the local boundary layer thickness.

We search for the hair length of largest output sensitivity over $0.01 \leqslant \ell^* \leqslant 40$ and boundary layer shapes over $2.216 \leqslant H \leqslant 4.029$. To examine output sensitivity with respect to boundary layer shape, hair moment (11) is nondimensionalized by the reference moment, $Q\,A\,\ell$, and normalized by the dependence of C_m on the external flow velocity, U, through Re_0. When equation (6) is substituted into (11), this leads to the following nondimensional expression:

$$M^* = C_m\, Re_0^{2/3} = \frac{1}{\ell^{*2}} \int_0^{\ell^*} d^{*1/3}\, u^{*4/3}\, \xi^*\, \mathrm{d}\xi^*. \tag{16}$$

Similarly, the resultant shear force (13) is nondimensionalized by the reference force, $Q\,A$, and normalized by its dependence on U to give

$$F^* = C_s\, Re_0^{2/3} = \frac{1}{\ell^*} \int_0^{\ell^*} d^{*1/3}\, u^{*4/3}\, \mathrm{d}\xi^*. \tag{17}$$

Equations (16) and (17) are general nondimensional expressions for laminar boundary layer flows. Note that for the direct application of (16) and (17) to Falkner–Skan solutions, we may rescale hair length and wall normal distance by δ (15), a specific measure of boundary layer thickness for Falkner–Skan flow, to obtain the following expressions that are equivalent to equations (16) and (17) above:

$$M^* = \left(\frac{\delta}{\ell}\right)^2 \int_0^{\ell/\delta} d^{*1/3}\, f'^{4/3}\, \eta\, \mathrm{d}\eta \tag{18}$$

and

$$F^* = \left(\frac{\delta}{\ell}\right) \int_0^{\ell/\delta} d^{*1/3}\, f'^{4/3}\, \mathrm{d}\eta. \tag{19}$$

Equations (18) and (19) are used in the following sections to compute the hair output and sensitivity.

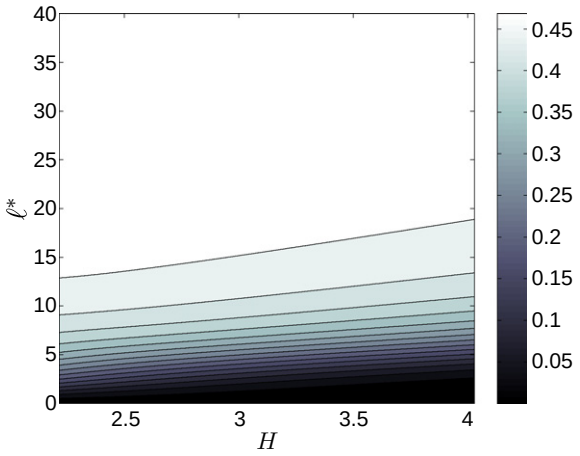

Figure 4. M^* as a function of ℓ^* and H for a hair sensor with uniform cross-section.

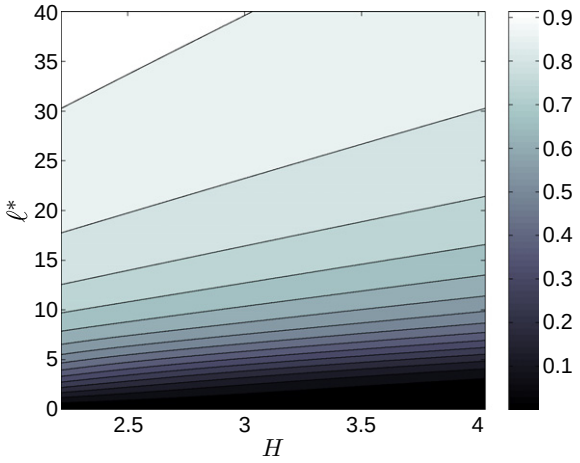

Figure 5. F^* as a function of ℓ^* and H for a hair sensor with uniform cross-section.

3.1. Hairs with uniform cross-section

This section contains the output and sensitivity of hairs with a uniform cross-section of $d = d_0 = 10\,\mu$m. Figures 4 and 5 are contour plots of M^* and F^* versus $\ell^* = \ell/\delta_2$ and H, respectively. The lines in figures 4 and 5 represent iso-moment and iso-shear contours, which trace paths of increasing ℓ^* as H increases from 2.216 to 4.029. The direction of the iso-output contours is an outcome of the flow changing from a situation where motion in the downstream direction is accelerated by a decreasing pressure gradient, to one where downstream motion is impeded by an increasing pressure gradient. For a hair mounted within the boundary layer, an increase in H corresponds to a decrease in nondimensional incident flow velocity, u/U (see figure 3). It follows that the iso-output contours follow paths of increasing length to supplement the output loss as H increases.

The sensitivity of the moment and shear force with respect to boundary layer shape is given by

$$S_{M^*} = \frac{\partial M^*}{\partial H} \tag{20}$$

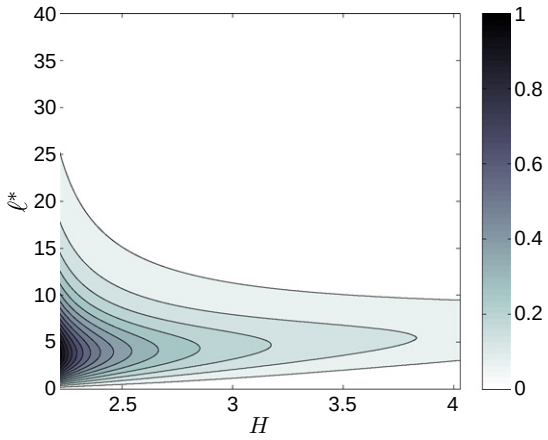

Figure 6. S_{M^*} normalized as a function of ℓ^* and H for a hair sensor with uniform cross-section.

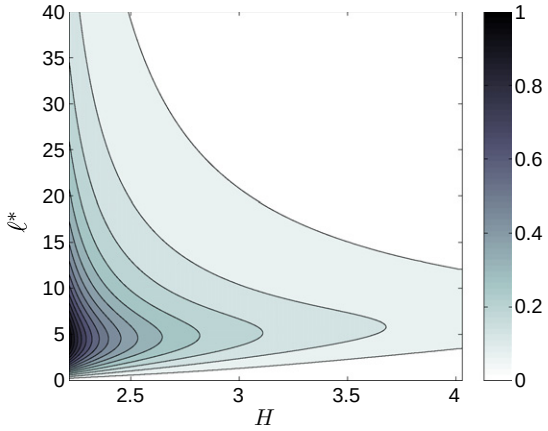

Figure 7. S_{F^*} normalized as a function of ℓ^* and H for a hair sensor with uniform cross-section.

and

$$S_{F^*} = \frac{\partial F^*}{\partial H}, \tag{21}$$

respectively. Output sensitivities (20) and (21) were computed over $2.216 \leqslant H \leqslant 4.029$ and $0 \leqslant \ell^* \leqslant 40$ with finite difference approximations, where the grid over H was sufficiently refined for grid independence. Figures 6 and 7 contain contour plots of the normalized moment and shear force sensitivities.

Here, we plot normalized sensitivity values for comparison to results contained the following section, where the effect of hair shape on output sensitivity is considered.

As conjectured at the beginning of this section, figures 6 and 7 show that output sensitivity decreases as hairs become much larger or much smaller than the boundary layer thickness (i.e. $\ell \gg \delta_2$ or $\ell \ll \delta_2$). The largest sensitivities over $2.216 \leqslant H \leqslant 4.029$ are observed for hair lengths roughly three to ten times the momentum thickness, with the global maximum sensitivity occurring near $\ell^* = 5$.

While the above sensitivity plots show that the largest sensitivities occur roughly over $3 < \ell^* < 10$, it does not provide a single relative hair length that overall is most

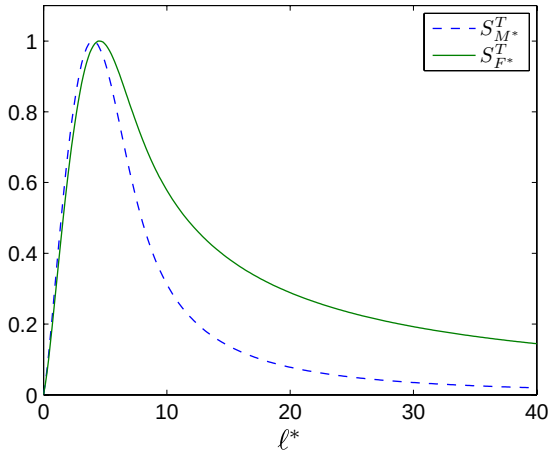

Figure 8. Normalized total sensitivity of hair, $S^T_{M^*}$ and $S^T_{F^*}$, with a uniform diameter as a function of ℓ^*.

sensitive to H. To this end, we also compute the following *total* output sensitivities over $2.216 \leqslant H \leqslant 4.029$ defined as

$$S^T_{M^*} = \int_{H_{\min}}^{H_{\max}} \frac{\partial M^*}{\partial H}\,\mathrm{d}H = M^*|_{H=4.029} - M^*|_{H=2.216} \quad (22)$$

and

$$S^T_{F^*} = \int_{H_{\min}}^{H_{\max}} \frac{\partial F^*}{\partial H}\,\mathrm{d}H = F^*|_{H=4.029} - F^*|_{H=2.216}. \quad (23)$$

Note that due to the monotonic behavior of M^* and F^* with respect to H, the total sensitivities (22) and (23) are equal to the difference between the maximum and minimum output moment and shear force values.

When $S^T_{M^*}$ and $S^T_{F^*}$ are plotted against ℓ^* (figure 8), global maximum values for moment and shear occur at $\ell^* = 4.02$ and $\ell^* = 4.56$, respectively.

We shall further refer to lengths of maximum total sensitivity as *optimal* and denote their values for output moment and shear with the subscript $(\cdot)_{M^*}$ and $(\cdot)_{F^*}$, respectively.

Nondimensional hair lengths scaled by the Falkner–Skan boundary layer thickness, δ (15), result in optimal values of $(\ell/\delta)_{M^*} = 2.10$ and $(\ell/\delta)_{F^*} = 2.40$. As H decreases from 4.029 to 2.216 the optimal hair lengths increase from 43.7% to 87.5% of δ_{99} for moment and from 50.0% to 100.0% of δ_{99} for shear force.

Finally, we note that as the relative hair lengths move from their optimal values in figure 8, output sensitivity sharply decreases, indicating that hair length is a critical geometric parameter for detecting changes in boundary layer shape.

3.2. Hairs with linearly tapered cross-section

Bat hair receptors have nonuniform cross-sections that are thickest at their base and taper to smaller diameters toward their tip (see figure 1 and [10]). As hair receptor lengths may be adapted for maximum output sensitivity, so may hair receptor shape. In this section, we provide a sensitivity analysis, similar to section 3.1, for hairs with linearly tapered cross-section.

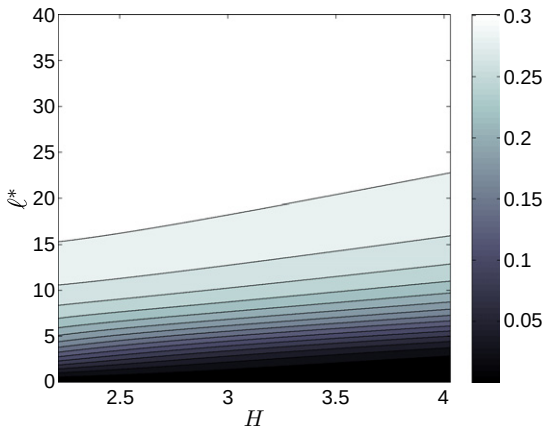

Figure 9. M^* as a function of ℓ^* and H for a hair sensor with linearly tapered cross-section.

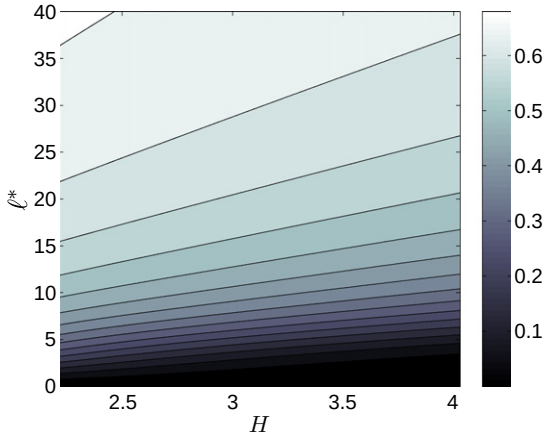

Figure 10. F^* as a function of ℓ^* and H for a hair sensor with linearly tapered cross-section.

Hair diameter as a function of hair longitudinal position may be expressed as

$$d(\xi) = d_0 \times \left(1 - \frac{\xi}{\ell}\right)^{\frac{1}{p}} \quad (24)$$

where d_0 is a reference hair diameter, and p is a hair shape index [38]. Here, we take $d_0 = 1 \times 10^{-5}\,\mu$m (the base diameter), and $p = 1$ for hairs shaped as linearly tapered cones.

Hair sensor outputs versus length ℓ^* and Hartree profile H showed similar trends to the output of uniform cross-section hairs (figures 9 and 10). Since linearly tapered hairs have less surface area than uniform cylinders of the same base diameter and length, the moment and shear output values in figures 9 and 10 are smaller than corresponding hair outputs with uniform cross-section (figures 4 and 5).

Figures 11 and 12 are contour plots of normalized output sensitivity, (20) and (21), as a function of ℓ^* and H, respectively. Similar to hairs with uniform cross-section, maximum sensitivities over H roughly occur over $3 < \ell^* < 10$. By comparing shear and moment sensitivities (figures 6–11 and figures 7–12), we find that the linearly tapered hair profile provides larger output sensitivities than hairs with uniform diameter.

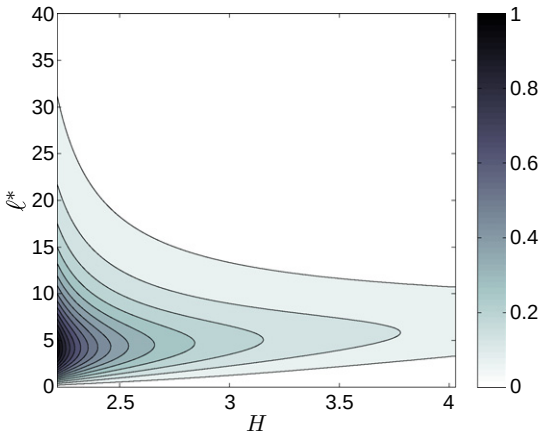

Figure 11. S_{M^*} normalized as a function of ℓ^* and H for a hair sensor with linearly tapered cross-section.

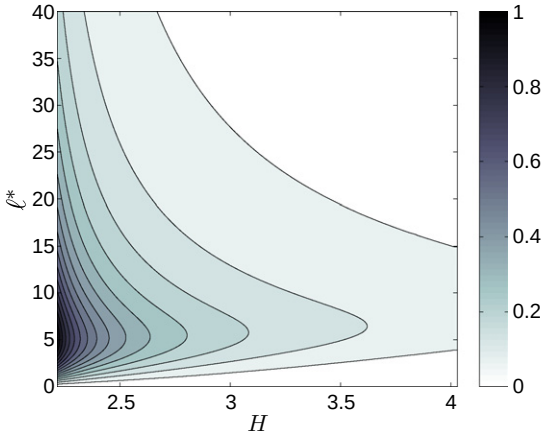

Figure 12. S_{F^*} normalized as a function of ℓ^* and H for a hair sensor with linearly tapered cross-section.

The normalized total sensitivities (22) and (23) show distinct optimal lengths (figure 13) of $\ell^*_{M^*} = 4.42$ and $\ell^*_{F^*} = 5.09$.

For hair length scaled by the Falkner–Skan boundary layer thickness, δ, optimal hair lengths occur at $(\ell/\delta)_{M^*} = 2.30$ and $(\ell/\delta)_{F^*} = 2.75$. As H decreases from 4.029 to 2.216, the optimal hair lengths increase from 47.9% to 94.6% of δ_{99} for moment and from 57.3% to 115.0% of δ_{99} for shear force.

The 15% extension of the optimal tapered hair length past δ_{99} for $H = 2.216$ is not completely unexpected. Although increasing a linearly tapered hair length beyond the boundary layer thickness creates an output contribution from the external flow, an increase in the diameter subject to the boundary layer profile also occurs (note that this cannot be said for hairs with uniform cross-section). Thus, for a certain length beyond the boundary layer, loss of output sensitivity from the contributions by the external flow is outweighed by the advantage of an increase in hair diameter within the boundary layer.

Comparing the sensitivity plots in the current and former section, it appears that hair shape can affect hair output sensitivity. This leads to the question of an optimal hair

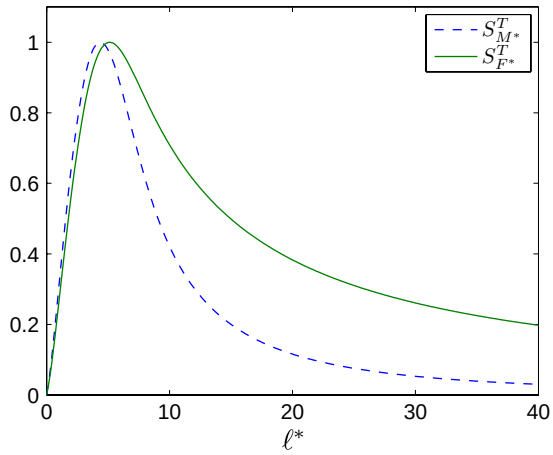

Figure 13. Sensitivity of hair, S_{M^*} and S_{F^*}, with a linearly tapered diameter as a function of ℓ^*.

shape for detecting fluctuations in the boundary layer shape. Interestingly, Kumagai *et al* found a similar 'square-root cone' shape among flow sensitive hairs on the cricket and cockroach [38]. In terms of equation (24), they computed a mean shape index and standard deviation of $1.91 \pm .30$ based on 16 hair samples from crickets, and $p = 2.22$ for the cockroach (too few cockroach hair samples were made for a standard deviation). Although 'evolutional optimization' was the suggested cause of the similarly shaped hairs, an explanation for the square-root cone shape was left as an open problem. Given the influence of hair shape on output sensitivity demonstrated here, hair output sensitivity appears to be a plausible influence responsible for the adaptation of hair receptor shape.

When the sensitivity analysis of sections 3.2 and 3.1 was applied for the cricket shape index, $p = 1.91$, the resulting sensitivities were greater than the uniform cross-section shape, but less than the linear cone shape. This result is not unexpected, since the Falkner–Skan boundary layer shapes are likely a poor description of the actual boundary layer profiles for which cricket and cockroach hairs may be adapted. Since hair receptors of the cricket and cockroach are used for predator avoidance [39–43], with an adequate characterization of the boundary layer flows due to the presence of predators, the hair shape index determined by Kumagai *et al* may provide greater output sensitivities than uniform, linearly tapered, and potentially many other hair shapes.

The results presented in sections 3.1 and 3.2 provide insight into artificial hair sensor design and integration into micro-air-vehicles. For the detection of the boundary layer shape (as opposed to the external flow), hair length should be chosen based on *a priori* knowledge of the boundary layer thicknesses. The optimal values of ℓ^* determined herein serve as guidelines for ensuring hair output sensitivity. These values are summarized in the first two columns of table 1. Included in the third and fourth columns of table 1 are the optimal hair lengths with respect to δ (15). However, because δ depends on m and x, the meaning of these values is limited to self-similar flows where these parameters have meaning. Finally, the ranges of hair length relative to δ_{99} for $2.216 \leqslant H \leqslant 4.029$ are listed in the last two columns.

Table 1. Summary of optimal relative hair lengths determined herein for hairs with uniform and linearly tapered cross-section.

Hair Shape	$(\ell/\delta_2)_{M^*}$	$(\ell/\delta_2)_{F^*}$	$(\ell/\delta)_{M^*}$	$(\ell/\delta)_{F^*}$	$(\ell/\delta_{99})_{M^*}$	$(\ell/\delta_{99})_{F^*}$
Uniform	4.02	4.56	2.10	2.40	0.437–0.875	0.500–1.00
Tapered	4.42	5.09	2.30	2.75	0.479–0.946	0.573–1.15

Table 2. Measured bat wing hair receptor lengths and optimal hair lengths computed from bat wing and flight measurements.

Species	Air speed (m s^{-1})	Average wing chord (m)	Measured hair length (μm)	Computed hair length (μm)
Pteropus poliocephalus	4.0–8.6[a] [44]	0.151 [7]	4000[b] [11]	100–3100
Glossophaga soricina	2.7–7.8 [45]	0.079 [46]	150–1000[c]	100–2600
Eptesicus fuscus	3.6–9.2 [47]	0.102	100–2000[c]	100–2600

[a] Enclosed speeds.
[b] Maximum length observed.
[c] Data courtesy of The Auditory Neuroethology Laboratory at The University of Maryland.

3.3. Comparison of optimal hair lengths with biological data

We now estimate the range of optimal hair lengths over the bat wing and compare these results to the range of hair receptor lengths measured on three different bat species. For each bat, the range of optimal hair lengths is computed by estimating the range of boundary layer thicknesses over the wing given flight-speed and chord-length data. The range of boundary layer thicknesses over the bat wing is estimated with the range of boundary layer thicknesses of Falkner–Skan solutions having surface lengths, L, equal to bat wing average chord-lengths, boundary layer shapes over $2.216 \leqslant H \leqslant 4.029$ and equal Reynolds numbers.

A Reynolds number for the forward flapping flight of the bats [29] is

$$Re_b = \frac{V_f\, L_c}{\nu}, \tag{25}$$

where V_f is the forward flight speed and L_c is the mean wing chord length, defined as the wing area divided by the wing span. For the Falkner–Skan flow we use the following Reynolds number:

$$Re = \frac{V\, L}{\nu}, \tag{26}$$

where V is a reference velocity taken as the external flow velocity evaluated at the trailing edge ($x = L$) of the no slip surface and L is the streamwise surface length. We then take $V = V_f$ and $L = L_c$ so that $Re_b = Re$.

Recall from table 1 that the optimal hair lengths relative to δ for linearly tapered hairs were computed as $(\ell/\delta)_{M^*} = 2.30$ and $(\ell/\delta)_{F^*} = 2.75$. With equation (15) for δ and V_f and L_c substituted for V and L, the dimensional optimal hair lengths are evaluated as

$$\ell_{M^*} = 2.30\sqrt{\frac{2}{m+1}\,\frac{\nu\, x}{U}} \quad \text{and} \quad \ell_{F^*} = 2.75\sqrt{\frac{2}{m+1}\,\frac{\nu\, x}{U}}, \tag{27}$$

respectively, where $U = V_f\,(x/L_c)^m$ and $m = \beta/(2-\beta)$.

The bat species, their range of forward flight speeds, values of their mean wing chord lengths and available data for their hair receptor lengths are listed in the first four respective columns of table 2. The fifth column contains the range of optimal hair lengths for both moment and shear outputs for $-0.199 \leqslant \beta \leqslant 1.0$, $V_{f,\min} \leqslant V_f \leqslant V_{f,\max}$ and $0.01\,L_c \leqslant x \leqslant 0.99\,L_c$. On an order of magnitude basis, the range of computed hair lengths is in agreement with the range of measured values for each bat. Considering that bat wing hair receptors are distinctly smaller in length and diameter than pelagial hair, the agreement between computed and measured hair lengths suggests that bat wing hair receptors are adapted for detecting changes in laminar boundary layer shape.

Note that dimensional optimal hair length (27) is a function of boundary layer shape (represented through β), flight speed V_f and hair position on the wing (or the Reynolds number at the hair location). While flight speed and boundary layer shape can vary during flight, hair position on the wing remains constant. Thus, for the detection of changes in laminar boundary layer shape, an optimal hair length may be determined based on *a priori* knowledge of the laminar boundary layer flow and will always be a compromise between flight speeds and shape factors.

The detection of boundary layer flows with multiple sensors located at different locations leads to a distribution of hairs with varying lengths over the lift surface. The equations for dimensional hair length in Falkner–Skan flows provide an expression for length distribution, $\ell \propto x^{1/2}$. Furthermore, the hair sensor length and distribution for any aircraft where flight performance relies on attached boundary layer flows could be determined with knowledge of the momentum thickness over the wing. This information is presently available through numerous computer programs, such as the XFOIL software [48], and through existing data in the literature.

The actual three-dimensional low-Reynolds number flows ($Re_f \sim 10^5$ or less) over bat wings during flapping flight exhibit other aerodynamically important flow phenomena that

are not as simple to analyze as two-dimensional laminar boundary layers. One such phenomenon is the leading edge vortex (LEV) which has been identified as a lift enhancement mechanism (see [29] and the references therein). Sterbing-D'Angelo *et al* hypothesized that wing regions affected by vortices would show specialization in the somatosensory cortex and that hair receptor removal in these regions would affect flight behavior [10]. Their studies showed a significant representation of the entire wing surface in the somatosensory cortex. When hair receptors were removed from the trailing edge, bats showed wider turns and higher average speeds. Although these results suggest that hair receptors provide airflow feedback during flight, it remains to be seen whether such feedback is specialized for vortex detection. Still, apart from this observation, to our knowledge no further evidence has been provided linking LEV detection to bat hair receptors.

Finally, we remark that turbulence is another aerodynamically important phenomenon for which bat hair receptors may have adapted. Although the question of turbulent flows is outside the scope of this work, just as the optimal hair length for laminar boundary layer detection is proportional to the boundary layer thickness, we anticipate a similar result with hold for turbulent boundary layers.

4. Summary

In this work, we studied the sensitivity of hair-like structures for the detection of changes in laminar boundary layer shape. A quasi-steady model relating the boundary layer shape to the resultant moment and shear force at the base of the hair was developed. The hair model was nondimensionalized using momentum thickness as a length scale and the resultant moment and shear force at the base of the hair (output) were computed for boundary layer shapes described by the Falkner–Skan equations.

Hair output sensitivity decreased as hair length became much larger or much smaller than the boundary layer thickness, while hairs with lengths approximately four to five times the momentum thickness provided the largest overall sensitivity.

We then defined an overall sensitivity measure (total sensitivity) for the range of boundary layer shapes considered. For hairs with uniform cross-section, the lengths of maximum total sensitivity were $4.02\,\delta_2$ and $4.56\,\delta_2$ for moment and shear force output, respectively. The optimal linearly tapered hair lengths were $4.42\,\delta_2$ and $5.09\,\delta_2$ for moment and shear force output, respectively.

The linearly tapered hair shape showed relatively larger output sensitivities than the hairs with uniform cross-section. Hair length was also shown to be a critical design parameter, as total output sensitivity sharply decayed as hair lengths moved away from their optimal values. Based on the influence of hair shape on output sensitivity, we submitted a working hypothesis that output sensitivity based on changes in boundary layer velocity profiles influenced the adaptation of hair receptor shape.

Finally, the boundary layer thickness over a bat wing was approximated with Falkner–Skan flow using physical and flight data of bats. On an order of magnitude basis, the range of optimal hair lengths computed from the analysis herein agreed with the range of measured hair receptor lengths on bat wings ($\sim$100–1000 μm). This result supports the hypothesis that bats use hair receptors for detecting changes in boundary layer velocity profiles.

Future work will focus on determining the optimal hair shape for laminar boundary layer detection and the detection of turbulence with hair receptors. The optimal placement and density of hair sensors for various low-Reynolds number flows of aerodynamic importance should also be studied for their effective integration on micro-air-vehicles and in control system designs.

Acknowledgments

The author would like to acknowledge Mark Drela for his initial suggestion of a quasi-steady hair model for optimal hair length studies and his insight during the revision process. Kenny Breuer, Dan Riskin, John Singler, Belinda Batten and Adam Rutkowski also provided helpful suggestions during the revision process. The author also thanks the anonymous reviewers for their suggestions, which ultimately led to a more complete and thorough study. Finally, the author would like to thank Sharon Swartz, Cynthia Moss, Susanne Sterbing-D'Angelo and Janna Barcelo for their direction, insight and interesting discussions regarding bat wing hair receptors. This research was supported in part by the Air Force Office of Scientific Research through grants FA9550-05-1-0041 and FA9550-07-1-0540.

References

[1] Winter Y and von Helversen O 1998 The energy cost of flight: Do small bats fly more cheaply than birds? *J. Comp. Physiol.* B **168** 105–11

[2] Tian X, Iriarte-Diaz J, Middleton K, Galvao R, Israeli E, Roemer A, Sullivan A, Song A, Swartz S and Breuer K 2006 Direct measurements of the flight kinematics and dynamics of bat flight *Bioinsp. Biomim.* **1** S10–18

[3] Swartz S M, Groves M S, Kim H D and Walsh W R 1996 Mechanical properties of bat wing membrane skin *J. Zool. Lond.* **239** 357–78

[4] Swartz S, Bishop K and Ismael-Aguirre M F 2005 Functional and evolutionary ecology of bats: implications for flight performance *Functional and Evolutionary Ecology of Bats* (Oxford: Oxford University Press)

[5] Vaughan T A 1970 The skeletal system *The Biology of Bats* vol 1 (New York: Academic) pp 98–139

[6] Swartz S M 1997 Allometric patterning in the limb skeleton of bats: implications of the mechanics and energetics of powered flight *J. Morphol.* **234** 277–94

[7] Swartz S M, Bennett M B and Carrier D R 1992 Wing bone stresses in free flying bats and the evolution of skeletal design for flight *Nature* **359** 726–9

[8] Zook J M and Fowler B C 1982 Central representation of a specialized mechanoreceptor array in the wing of the bat *Neurosci. Abstr.* **8** 38

[9] Zook J M 2005 The neuroethology of touch in bats: cutaneous receptors of the wing *Neurosci. Abstr. 78.21*

[10] Sterbing-D'Angelo S, Chadha M and Moss C 2008 Representation of the wing membrane in somatosensory cortex of the bat *Eptesicus fuscus Neurosci. Abstr. 370.4*

[11] Crowley G and Hall L 1994 Histological observations on the wing of the grey-headed flying-fox (*Pteropus poliocephalus*) (Chiroptera: Pteropodidae) *Aust. J. Zool.* **42** 215–31

[12] Zook J 2006 Somatosensory adaptions of flying mammals *Evolution of Nervous Systems* vol 3 (Oxford: Academic) pp 215–26

[13] Barth F, Wastl U, Humphrey J and Devarakonda R 1993 Dynamics of arthropod filiform hairs: II. Mechanical properties of spider trichobothria (*Cupiennius salei* Keys) *Phil. Trans. R. Soc.* B **340** 445–61

[14] Devarakonda R, Barth F and Humphrey J 1996 Dynamics of arthropod filiform hairs: IV. Hair motion in air and water *Phil. Trans. R. Soc.* B **351** 933–46

[15] Humphrey J and Barth F 2008 *Medium Flow-Sensing Hairs: Biomechanics and Models* (*Advances in Insect Physiology* vol 34) (New York: Academic) pp 1–80

[16] Barth F 2000 How to catch the wind: spider hairs specialized for sensing the movement of air *Naturwissenschaften* **87** 51–8

[17] Dickinson B T, Singler J R and Batten B A 2008 The detection of unsteady flow separation with bioinspired hair-cell sensors *Proc. of the 26th AIAA Aerodynamic Measurement and Ground Testing Conf.*

[18] Dickinson B 2009 Detecting fluid flows with bioinspired hair sensors *PhD Thesis* Oregon State University, Corvallis, OR

[19] Joshi S S, Speyer J L and Kim J 1997 A systems theory approach to the feedback stabilization of infinitesimal and finite-amplitude disturbances in plane Poiseuille flow *J. Fluid Mech.* **332** 157–84

[20] Högberg M, Bewley T R and Henningson D S 2003 Linear feedback control and estimation of transition in plane channel flow *J. Fluid Mech.* **481** 149–75

[21] Chevalier M, Hœpffner J, Åkervik E and Henningson D S 2007 Linear feedback control and estimation applied to instabilities in spatially developing boundary layers *J. Fluid Mech.* **588** 163–87

[22] Dickinson B T, Singler J R and Batten B A 2006 Modeling of bioinspired sensors for flow separation detection for micro air vehicles *Proc. of the 3rd AIAA Flow Control Conf.*

[23] Coombs S 2001 Smart skins: information processing by lateral line flow sensors *Auton. Robots* **11** 255–61

[24] Liu C 2007 Micromachined biomimetic artificial hair cell sensors *Bioinsp. Biomim.* **2** 162–9

[25] Abdulrahim M, Garcia H and Lind R 2005 Flight characteristics of shaping the wing membrane of a micro air vehicle *J. Aircr.* **42** 131–7

[26] Humphrey J, Devarakonda R, Iglesias R and Barth F 1993 Dynamics of arthropod filiform hairs: I. Mathematical hair modeling of the hair and air motions *Phil. Trans. R. Soc.* B **340** 423–44

[27] Barth F, Humphrey J, Wastl U, Halbritter J and Brittinger W 1995 Dynamics of arthropod filiform hairs: III. Flow patterns related to air movement detection in a spider (*Cupiennius salei* KEYS) *Phil. Trans. R. Soc.* B **347** 397–412

[28] Steinmann T, Casas J, Krijnen G and Dangles O 2006 Air-flow sensitive hairs: Boundary layers in oscillatory flows around arthropod appendages *J. Exp. Biol.* **209** 4398–408

[29] Shyy W, Lian Y, Tang J, Viieru D and Liu H 2008 *Aerodynamics of Low Reynolds Number Flyers* (Cambridge: Cambridge University Press)

[30] Billone M and Raynor S 1973 Transmission of radial shear forces to cochlear hair cells *J. Acoust. Soc. Am.* **54** 1143–56

[31] Aranyosi A J and Freeman D M 2004 Sound-induced motions of individual cochlear hair bundles *Biophys. J.* **87** 3536–46

[32] Nam J H, Cotton J R and Grant J W 2005 Effect of fluid forcing on vestibular hair bundles *J. Vestib. Res.* **15** 263–78

[33] Davis J 1987 *Dynamics of Continuous Media* (London: Macmillan)

[34] Feughelman M 1997 *Mechanical Properties and Structure of Alpha-Keratin Fibres* (Sydney: University of New South Wales Press)

[35] Prandtl L 1952 *Essentials of Fluid Dynamics* (New York: Hafner)

[36] Keller H B and Cebeci T 1971 Accurate numerical methods for boundary layer flows: I. Two dimensional laminar flows *Proc. 2nd Int. Conf. Numer. Meth. Fluid Dyn. (Lecture Notes in Physics)* (Berkley, CA: Springer)

[37] Schlichting H and Gersten K 2000 *Boundary Layer Theory* (Berlin: Springer)

[38] Kumagai T, Shimozawa T and Baba Y 1998 The shape of wind-receptor hairs of cricket and cockroach *J. Comp. Physiol.* A **183** 187–92

[39] Camhi J, Tom W and Volman S 1978 The escape behavior of cockroach *Periplaneta americana*: II. Detection of natural predators by air displacement *J. Comp. Physiol* **128** 203–12

[40] Camhi J 1980 The escape system of cockroach *Sci. Am.* **243** 144–56

[41] Gnatzy W and Hußlein R 1986 Digger wasp against crickets: I. Receptor involved in the antipredator strategies of the prey *Naturwissenschaften* **73** S.212

[42] Gnatzy W and Hustert R 1989 Mechanoreceptors in behavior *Cricket Behavior and Neurobiology* (Ithaca, NY: Cornell University Press) pp 198–266

[43] Tauber E and Camhi J 1995 The wind-evoked escape behaviour of the cricket *Gryllus bimaculatus*: integration of behavioral elements *J. Exp. Biol.* **198** 1895–907

[44] Carpenter R E 1985 Flight physiology of flying foxes, *Pteropus poliocephalus J. Exp. Biol.* **114** 619–47

[45] Akins J B, Kennedy M L, Schnell G D, Sánchez-Hernández C, Romero-Almaraz M, Wooten M C and Best T L 2007 Flight speeds of three species of neotropical bats: Glossophaga soricina, Natalus stramineus, and Carollia subrufa *Acta Chiropterol.* **9** 477–82

[46] Norberg U M 1981 Allometry of bat wings and legs and comparison with bird wings *Phil. Trans. R. Soc.* B **292** 359–98

[47] Patterson A P and Hardin J W 1969 Flight speeds of five species of vespertilionid bats *J. Mammal.* **50** 152–3

[48] Drela M 1989 An analysis and design system for low Reynolds number airfoils *Proc. of the Conf. on Low Reynolds Number Aerodynamics*